Supplementary Information

Desktop Inkjet Printing of Foldable Metasurface Antenna on Paper Substrates

Rupesh Pawar[1], Soumya Chakravarty[2], Tapas Chakravarty[2]* and Venugopal Santhanam[1]*

[1] Department of Chemical Engineering, Indian Institute of Science, Bangalore-560012, India.

[2] TCS Research, IIT Kharagpur Research Park- NSTP Plot No. -III-B/12, Action Area III, New Town, Kolkata-700160, India.

*E-mail: tapas.chakravarty@tcs.com, svgpal@iisc.ac.in

S1. Calibration plot for ICP-OES analysis

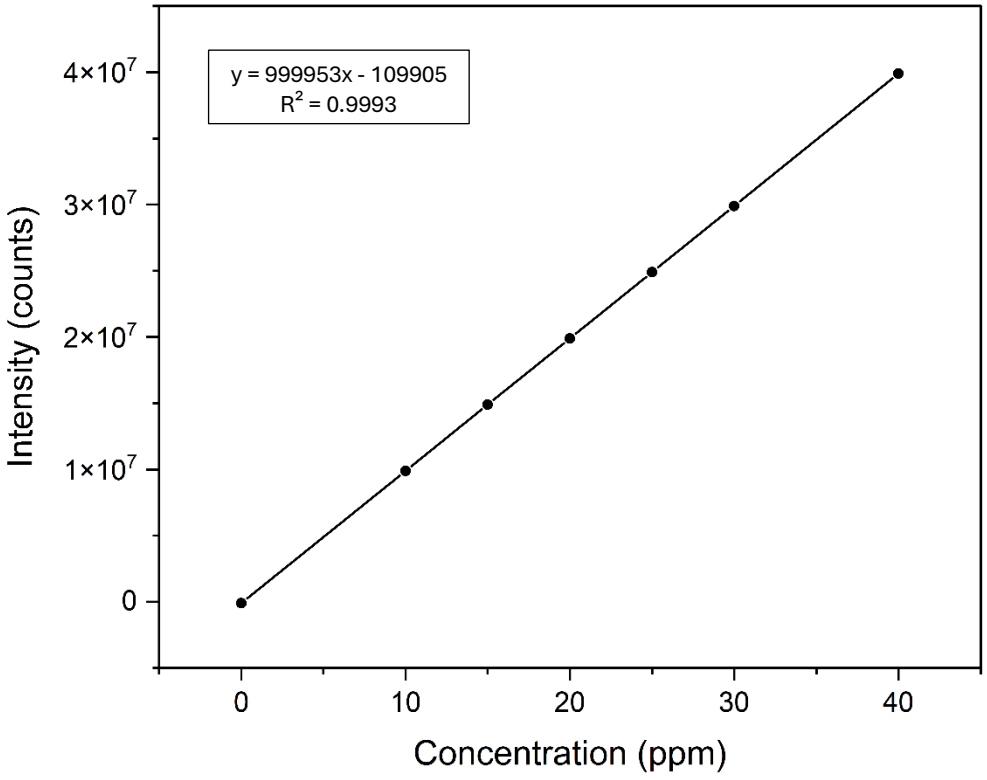

Fig. S1: Calibration plot and prediction interval for ICP – OES analysis.

Concentration (ppm)	Y[Intensity] (cts)	Y(pred)-E (cts)	Y(pred)+E (cts)
0	-109921.2	-109921.7	-109920.7
10	9889617.0	9889616.6	9889617.4
15	14889386.1	14889385.8	14889386.5
20	19889155.2	19889154.9	19889155.5
25	24888924.3	24888923.9	24888924.6
30	29888693.4	29888693.0	29888693.8
40	39888231.6	39888231.1	39888232.1

To determine the prediction interval, a calibration plot was constructed using a series of silver standards (0, 5, 10, 15, 20, 25, and 30 ppm), each prepared in triplicate with $AgNO_3$ in 2% HNO_3. The prediction interval quantifies the uncertainty associated with predicted concentration values and is calculated using the following expression[1]:

$$\hat{y} - E < y < \hat{y} + E$$

where:

$$E = \frac{t_{\alpha/2} * standard\ error}{s} * \sqrt{1/N + 1/n + (x^* - x_{mean})^2 / \sum (x_i - x_{mean})^2}$$

N: number of repeat measurements made on the standard solution (N = 3 for measurement repeated thrice)

n: number of paired calibration points

s: slope of the calibration curve

x*: the value of a particular standard's concentration

x_{mean}: average of the xi values

$t_{\alpha/2}$: Student t value for the 95% conference with n-2 degrees of freedom

S2. Porosity Calculation Methodology

The porosity of the deposited silver (Ag) layers was determined by comparing the calculated apparent density (ρ_{app}) of the coating with the known theoretical density of bulk silver ($\rho_{bulk,Ag}$).

a. Apparent Density Calculation

The apparent density of each deposited layer was calculated from the experimental mass loading (m_A, in mg/cm^2) and the deposition thickness (t, in μm). The apparent density is the ratio of the mass loading to the thickness:

$$\rho_{app} = \frac{m_A}{t}$$

To ensure correct unit conversion from the measured units to a standard density unit (g/cm^3), a conversion factor of 10 is applied:

$$\rho_{app}(g/cm^3) = \frac{m_A(mg/cm^2)}{t\ (\mu m)} \times 10$$

Example calculation using the lowest loading:

$$\rho_{app}(g/cm^3) = \frac{0.64(mg/cm^2)}{4.4\ (\mu m)} \times 10 = 1.455\ g/cm^3$$

b. Porosity Calculation

The porosity ε, expressed as a percentage, represents the fraction of void volume within the coating. It was calculated by comparing the apparent density (ρ_{app}) to the theoretical density of bulk silver, which is taken as $\rho_{bulk,Ag} = 10.49$ g/cm³

The formula used is:

$$\varepsilon(\%) = \left(1 - \frac{\rho_{app}}{\rho_{bulk,Ag}}\right) \times 100\%$$

Example calculation:

$$\varepsilon(\%) = \left(1 - \frac{1.455\ g/cm^3}{10.49\ g/cm^3}\right) \times 100\% = 86.1\%$$

Additionally, the Relative Density (or Material Volume Fraction) was calculated. This represents the percentage of the coating's volume occupied by silver nanostructure material compared to bulk silver.

Relative Density (%) = 100 - ε(%)

c. Summary of Calculated Data

The calculations were applied to each sample, as summarized in Table S2. The reported thickness values represent the mean of measurements, and the uncertainty corresponds to the standard deviation of those measurements. The average porosity and its standard deviation were calculated from the set of four individual porosity values.

Table S2: Summary of Porosity Calculation Data

Loading (mg/cm2)	Deposition Thickness (µm)	Porosity(%)	Relative silver nanostructure Density (%)
0.64	4.4 ± 0.6	86.1	13.9
1.28	9.4 ± 0.7	87	13.0
1.6	11.2 ± 0.8	86.4	13.6
2.56	17.0 ± 0.9	85.6	14.4
Average		**86.3**	**13.7**
Standard Deviation		**0.6**	**0.6**

Table S3. A comparative analysis of different literatures from the manufacturability aspect

Ref	Process	Antenna Prototype	Antenna Type	Frequency (GHz)	Gain (dBi)	Substrate	Remarks
(Lei et al., 2025)	Photolithographically pattern the stainless-steel screen + Screen-print copper nanoparticle ink + thermal treatment		straight dipoles, meandering dipoles, circular disc monopoles, and 2×1 monopole antenna arrays with CPW feeding	24	-	Polyimide film, Willow glass ribbon, Alumina ribbon ceramic	Subtractive Complex Processing steps (Stable Ink formulation, Thermal Processing, Lithography)
(Muhammad et al., 2024)	Manual fabrication using copper conductive tape adhered to paper substrates		metasurface-backed microstrip patch antenna	5.2-12.5	2	Paper	An additive process, but poor reproducibility due to manual patterning and limited to simple designs
(Yang et al., 2024)	Inkjet-printing(PeJet-DP500 microelectronics printer) of silver-nano ink followed by plasma sintering	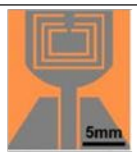	circular-monopole variant with coplanar-waveguide feed and three nested C-slot notches.	2.9–10.61	5.5	PET	An additive process, but requires Complex ink formulation and sintering steps, as well as dedicated material printer setup
(Hamlbar Gerami et al., 2024)	Conventional PCB fabrication		Metasurface slot antenna	23-31	9.43	RO4003C and RT/duroid	A subtractive manufacturing process based on photolithography
(Ashraf et al., 2022)	Inkjet printing (Brother DCP-T310) using silver-nanoparticle conductive ink		metamaterial-loaded monopole antenna	2.4	0.6	Rogers RO3010 and photo-paper	An additive process, but requires Complex ink formulation and sintering steps
(Chakravarty et al., 2022)	photolithographic etching	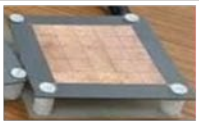	Probe-fed microstrip patch antenna with transmissive metasurface lens	5.8	5.38	FR-4 and RT-Duroid 5880	A subtractive manufacturing process based on photolithography
(Hongnara et al., 2018)	photolithographic etching	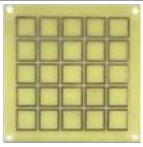	Slot-fed beam-steering metasurface antenna	2.40–2.50+-	8.69	FR-4	A subtractive manufacturing process based on photolithography
(Abutarboush & Shamim, 2018)	Inkjet printing (Dimatix DMP-2831) with silver nanoparticle-based ink followed by oven sintering	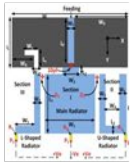	reconfigurable multiband antenna with switchable main, L-shaped, and U-shaped radiators	1.9-3.4	~2	resin-coated photo paper	An additive process, but requires Complex ink formulation and sintering steps, as well as dedicated material printer setups
(Kim et al., 2012)	Inkjet-printing (Dimatix) of conductive nano-silver ink followed by thermal sintering		Microstrip monopole backed by inkjet-printed EBG array forming AMC reflector	2.36–2.61	0.95	photo-paper	An additive process, but requires Complex ink formulation and sintering steps, as well as dedicated material printer setups
This work	Print- Expose- Develop	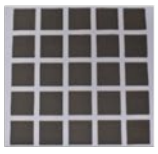	Dual-layer transmissive metasurface lens (5×5 square patch array) + microstrip patch feed	4	6.1	Paper	An additive process using an office desktop printer and aqueous salt precursor solutions. Photographic chemistry that was widely used in 20th century

References-

1. Ogunnaike BA. Random Phenomena, 1st ed., CRC Press, Boca Raton, 2009. https://doi.org/10.1201/b17197.

2. Abutarboush, H. F., & Shamim, A. (2018). A Reconfigurable Inkjet-Printed Antenna on Paper Substrate for Wireless Applications. IEEE Antennas and Wireless Propagation Letters, 17(9), 1648–1651. https://doi.org/10.1109/LAWP.2018.2861386

3. Ashraf, F. Bin, Alam, T., Islam, M. T., Singh, M. J., Misran, N. B., & Islam, M. T. (2022). Inkjet printed metamaterial loaded antenna for WLAN/WiMAX applications. Computers, Materials and Continua, 71(2), 2271–2284. https://doi.org/10.32604/cmc.2022.021751

4. Chakravarty, S., Kumar, A., Chakravarty, T., Pal, A., & Ghatak, R. (2022). A Metasurface-Enabled Lens Antenna Demonstrating Electromechanical Beam-Tilting for 5G Applications. 2022 National Conference on Communications, NCC 2022, 30–35. https://doi.org/10.1109/NCC55593.2022.9806743

5. Hamlbar Gerami, H., Kazemi, R., & Fathy, A. E. (2024). Development of a metasurface-based slot antenna for 5G MIMO applications with minimized cross-polarization and stable radia-tion patterns through mode manipulation. Scientific Reports, 14(1). https://doi.org/10.1038/s41598-024-58794-1

6. Hongnara, T., Chaimool, S., Akkaraekthalin, P., & Zhao, Y. (2018). Design of Compact Beam-Steering Antennas Using a Metasurface Formed by Uniform Square Rings. IEEE Access, 6, 9420–9429. https://doi.org/10.1109/ACCESS.2018.2799551

7. Kim, S., Ren, Y. J., Lee, H., Rida, A., Nikolaou, S., & Tentzeris, M. M. (2012). Monopole an-tenna with inkjet-printed EBG array on paper substrate for wearable applications. IEEE Antennas and Wireless Propagation Letters, 11, 663–666. https://doi.org/10.1109/LAWP.2012.2203291

8. Lei, H., Patel, T., Lopez, J., & Devin MacKenzie, J. (2025). Screen-Printed Flexible Antennas for 24-GHz ISM Band and mmWave Applications. IEEE Journal on Flexible Electronics, 4(4), 138–145. https://doi.org/10.1109/JFLEX.2025.3560936

9. Muhammad, H. A., Abdulkarim, Y. I., Abdoul, P. A., Awl, H. N., Teksen, F. A., Alkurt, F. O. ̈zkan, Karaaslan, M., Bakır, M., & Appasani, B. (2024). A highly flexible and low-profile metasur-face antenna for wearable WBAN systems. Optik, 313. https://doi.org/10.1016/j.ijleo.2024.171974

10. Yang, W., Zhao, X., Guo, Z., Sun, H., & List-Kratochvil, E. J. W. (2024). A compact tri-notched flexible UWB antenna based on an inkjet-printable and plasma-activated silver nano ink. Scientific Reports, 14(1). https://doi.org/10.1038/s41598-024-62253-2